Petroleum Science 19 (2022) 2796–2809

Contents lists available at ScienceDirect

Petroleum Science

journal homepage: www.keaipublishing.com/en/journals/petroleum-science

Original Paper

A FEM-DFN model for the interaction and propagation of multi-cluster fractures during variable fluid-viscosity injection in layered shale oil reservoir

Chu-Hao Huang [a], Hai-Yan Zhu [a, *], Jian-Dong Wang [b], Jian Han [c], Guang-Qing Zhou [b], Xuan-He Tang [a]

[a] State Key Laboratory of Oil and Gas Reservoir Geology and Exploitation, Chengdu University of Technology, Chengdu, 610059, Sichuan, PR China
[b] Petroleum Engineering Technology Research Institute, Shengli Oilfield Company, SINIOPEC, Dongying, 257000, Shandong, PR China
[c] Chongqing Gas Field, Southwest Oil and Gas Field Company, PetroChina, Chongqing, 400021, PR China

ARTICLE INFO

Article history:
Received 4 March 2022
Received in revised form
11 June 2022
Accepted 13 June 2022
Available online 15 June 2022

Edited by Yan-Hua Sun

Keywords:
Shale oil reservoir
FEM-DFN model
Fracture propagation
Variable fluid-viscosity injection
Bedding planes

ABSTRACT

To investigate the height growth of multi-cluster fractures during variable fluid-viscosity fracturing in a layered shale oil reservoir, a two-dimensional finite element method (FEM)-discrete fracture network (DFN) model coupled with flow, stress and damage is proposed. A traction-separation law is used to describe the mixed-mode response of the damaged adhesive fractures, and the cubic law is used to describe the fluid flow within the fractures. The rock deformation is controlled by the *in-situ* stress, fracture cohesion and fluid pressure on the hydraulic fracture surface. The coupled finite element equations are solved by the explicit time difference method. The effects of the fracturing treatment parameters including fluid viscosity, pumping rate and cluster spacing on the geometries of multi-fractures are investigated. The results show that variable fluid-viscosity injection can improve the complexity of the fracture network and height of the main fractures simultaneously. The pumping rate of 15 m^3/min, variable fluid-viscosity of 3-9-21-36-45 mPa s with a cluster spacing of 7.5 m is the ideal treatment strategy. The field application shows that the peak daily production of the application well with the optimized injection procedure of variable fluid-viscosity fracturing is 171 tons (about 2.85 times that of the adjacent well), which is the highest daily production record of a single shale oil well in China, marking a strategic breakthrough of commercial shale oil production in the Jiyang Depression, Shengli Oilfield. The variable fluid-viscosity fracturing technique is proved to be very effective for improving shale oil production.

1. Introduction

Following shale gas, shale oil has become another alternative resource with large development potential in China. Shale oil reservoirs have obvious laminated structures with bedding planes, which results in variable *in-situ* stress and interbedded layer properties. To achieve a commercial well production rate, it is desirable to form the stimulated reservoir volume (SRV) covering multiple shale layers. However, the thin limestone interlayers embed in the organic-rich pay layer, shielding the hydraulic fractures to cross through limestone interlayers and connect to multiple pay layers. The microseismic monitoring results showed that the height of hydraulic fractures was much lower than the production-expected value, even if the pumping rate was rose to the best of field injection ability. Research has shown that the fracture growth in fracturing treatment is largely determined by fracturing fluid viscosity. Guo et al. (2019) illustrated that lower fluid viscosity is favorable to formation of shear fracture and larger length of fracture. Zhu et al. (2019) found that hydraulic fractures are easier to propagate to the interlayers under the condition of

* Corresponding author.
E-mail address: zhuhaiyan040129@163.com (H.-Y. Zhu).

https://doi.org/10.1016/j.petsci.2022.06.007

high fluid viscosity. Inspired by these findings, in this paper, we proposed a new technique called variable fluid-viscosity fracturing to implement the effective growth of hydraulic fractures in layered reservoir. However, so far, the effect of variable viscosity on the height growth behavior of hydraulic fractures has not been thoroughly studied. Therefore, it is a challenge to choose the appropriate treatment scheme under the condition of variable viscosity fracturing fluid.

In the past decades, many numerical methods have been developed to simulate the propagation behavior of fractures during hydraulic fracturing, including DFN (Zhu et al., 2021), FEM (Lu et al., 2015; Zhu et al., 2015, 2016), extended finite element method (XFEM) (Zeng et al., 2018), phase field method (PFM) (Miehe et al., 2015; Guo et al., 2018), element partition method (EPM) (Zhang et al., 2013, 2016; Wang and Zhang, 2020), boundary element method (BEM) (Rahman et al., 2002; Hossain and Rahman, 2008) and displacement discontinuity method (DDM) (Shou and Napier, 1999; Li et al., 2021). However, the methods have defects in dealing with interaction of multiple fluid-driven fractures. DDM is difficult to predict the close-spacing fracture behavior in inhomogeneity and anisotropy rock mass. XFEM has limitations for depicting the geometry of fracture network due to the complex local enrichment function. DEM treats rock mass as a combination of discrete blocks and can indirectly characterize the macro mechanical parameters of rock mass. FEM is suitable for heterogeneous materials with complex constitutive behavior and can solve the intersection and propagation of multiple fractures without utilizing enrichment shape function. However, FEM cannot capture the formation of new discontinuous structures during the fracture process.

By for, plenty of research focused on the effect of bedding planes on fracture height growth. Based on numerical simulations (Wang et al., 2015; Guo et al., 2017; Weng et al., 2018; Tang et al., 2019; Aimene et al., 2019; Xie et al., 2020) and laboratory investigations (Li et al., 2014, 2018; Bunger et al., 2015; Zou et al., 2017), they realized that bedding planes can greatly affect the ultimate fracture geometries. It is indicated that the existence of bedding planes can cause the hydraulic fractures to stop propagating, initiate shear fractures or create offsets along the interfaces (Zhang et al., 2007; Tang et al., 2018; Ju et al., 2019; Zhou et al., 2020). Although these results have revealed the interaction mechanism between hydraulic fractures and bedding planes to a certain extent, there are relatively few models that can quantitatively characterize the fracture geometries.

In this paper, a two-dimensional FEM-DFN model is developed to seek the interaction mechanism of hydraulic fractures and bedding planes and optimize appropriate fracturing treatment parameters for variable fluid-viscosity fracturing. Based on the model, numerical simulations around the height growth of multi-cluster fractures and the formation of the complex fracture network are presented. This paper is organized as follows.

Firstly, the principle of variable fluid-viscosity fracturing and modeling method is introduced in Section 2. Then, a model for describing the propagation of two-dimensional multi-cluster fractures is established and the results of the model are compared with the analytical model in Section 3. The effect of fracturing fluid viscosity, pumping rate and cluster spacing on fracture geometries and total fracture length is investigated in Section 4. Finally, the optimization results have been applied to a typical horizontal well in the Shengli Oilfield. The microseismic monitoring results of the well reveal that variable fluid-viscosity fracturing can effectively improve the height of the main fractures and the complexity of the fracture network. And the production data after fracturing show that the technique is conducive to improve well production.

2. FEM-DFN modelling method for the interaction and propagation of multi-cluster fractures

2.1. Brief introduction to variable fluid-viscosity fracturing technique

The horizontal bedding planes are widely distributed in shale oil reservoir, which make great difficulty for hydraulic fractures to connect multiple producing layers in fracturing treatment. Due to the limitation of field conditions, the adjustment of fluid viscosity is a more realistic way to improve the fracturing effect. Field application revealed that hydraulic fractures are difficult to cross through the bedding planes with low viscosity fracturing fluid. However, increasing the viscosity of fracturing fluid will greatly reduce the activated shear fractures, which is unfavorable to increase the complexity of fracture network. To solve this problem, we propose a new fracturing technique called variable fluid-viscosity fracturing. Fig. 1 shows the whole propagation process of the hydraulic fractures in height direction. Firstly, the low-viscosity fracturing fluid is used in the early stage of the variable viscosity fracturing treatment. The fractures are inclined to propagate in the horizontal direction, which can effectively improve the complexity of the fracture network in the fracturing layer. Then, the viscosity of fracturing fluid is increased gradually and the height direction changes into the dominant direction of fracture propagation. Finally, when the viscosity of fracturing fluid increases to a certain extent, the fracture could cross through the bedding planes, which ensures that the main fracture has sufficient height to connect with other pay layers.

2.2. Mathematical model

In this paper, we developed a FEM-DFN model to simulate the fracture geometries during variable fluid-viscosity fracturing. As shown in Fig. 2, the rock mass is discretized with meshes comprised of 3-noded triangular elements. And it is assumed that the elements are impervious. Then, the joint elements are inserted between arbitrary two adjacent triangular elements. The initial aperture of the joint elements is given to represent the permeability of the rock mass. The hydraulic fractures can growth along any possible paths within the constraints imposed by the mesh topology. Finally, the joint elements have been generated (the blue elements in Fig. 2). When the fluid flow into the elements, the permeability increases with the increase in the aperture of the joint elements. As a consequence, the seepage within fractures can be considered.

The dynamic equation during fracture propagation can be expressed as:

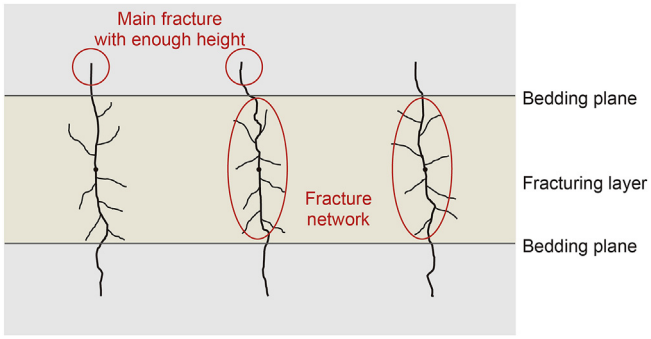

Fig. 1. Schematic of fracture geometry of variable fluid-viscosity fracturing.

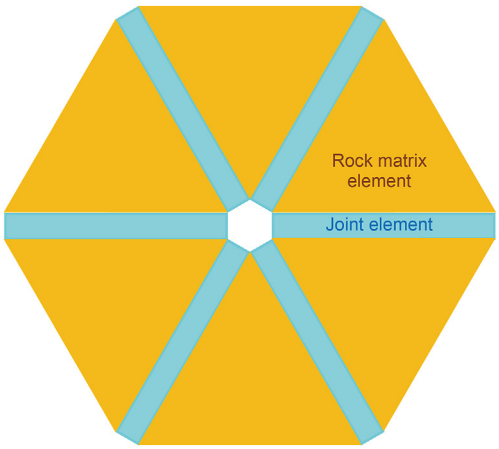

Fig. 2. Matrix element discretization and joint element inserting.

$$\mathbf{M}\ddot{x}+\mathbf{C}\dot{x}+\mathbf{K}(x)+\mathbf{F}_{\text{int}}(x)-\mathbf{F}_{\text{ext}}(x)-\mathbf{F}_{\text{c}}(x)=0 \tag{1}$$

where $\mathbf{M}$ is the mass matrix of all nodes; $\mathbf{C}$ is the damping matrix of all nodes; $\mathbf{K}$ is the stiffness matrix; $\mathbf{F}_{\text{int}}(x)$ is the vector of the internal load on fracture surface; $\mathbf{F}_{\text{ext}}(x)$ is the vector of external load; $\mathbf{F}_{\text{c}}(x)$ is the vector of the contact forces; x is the vectors of nodal displacement; $\dot{x}$ is the vectors of nodal velocity; and $\ddot{x}$ is the vectors of nodal acceleration.

The damping matrix $\mathbf{C}$ is given by:

$$\mathbf{C}=\mu\mathbf{I} \tag{2}$$

where μ is the constant damping coefficient; and $\mathbf{I}$ is the unit matrix. According to the single-degree-of-freedom point spring system, the constant damping coefficient is determined as (Munjiza, 2004):

$$\mu=2h\sqrt{\rho E} \tag{3}$$

where h is the length of the element; ρ is the density of the rock mass; and E is the elastic modulus of the rock mass. The stress and strain of the matrix elements are calculated by finite element method and the contact between adjacent matrix elements is addressed with discrete element method. So, the governing equations can be divided into two parts and solved separately:

$$\mathbf{M}\ddot{x}+\mathbf{C}\dot{x}+\mathbf{K}(x)=\mathbf{F}_{\text{ext}}(x) \tag{4}$$

$$\mathbf{H}\frac{\partial\mathbf{p}}{\partial t}+\mathbf{F}_{\text{int}}(x)=\mathbf{F}_{\text{ext}}(x) \tag{5}$$

where $\mathbf{H}$ is the concentrated volume matrix; and $\mathbf{p}$ is the vector of nodal pressure.

In our model, implicit difference solution is used to solute the governing equations to ensure the solution convergence. For each node, the velocity at time $t+1$ is determined as:

$$\dot{x}_{t+1}=\dot{x}_t+\ddot{x}_t\Delta t \tag{6}$$

where Δt is the integration time step. Then, the updated nodal position is obtained as:

$$x_{t+1}=x_t+\dot{x}_{t+1}\Delta t \tag{7}$$

In addition, the nodal pressure at time $t+1$ is determined as:

$$\mathbf{p}_{t+1}=\mathbf{p}_t+\frac{\partial\mathbf{p}}{\partial t}\Delta t \tag{8}$$

2.2.1. Fluid flow within fractures

As shown in Fig. 3, when a joint element breaks, the joint element becomes the flow channel within the fractures. When the fluid flows into the joint element, the fluid pressure is applied onto the fracture surfaces. The fluid is assumed to be incompressible, and cubic law is used to calculate the flow rate from Node 6 to Node 5:

$$q=-\frac{a^3}{12\nu_{\text{f}}}\frac{\Delta p}{L} \tag{9}$$

where q is the flow rate; a is the average aperture of the joint element; ν_{f} is the kinematic viscosity of the fluid; L is the length of the joint element; and Δp is the pressure difference between Node 6 and Node 5.

And the total pressure difference between Node 6 and Node 5 is given by:

$$\Delta p=p_6-p_5+\rho_{\text{w}}g(y_6-y_5) \tag{10}$$

where p_6 and p_5 are the fluid pressure at Node 6 and Node 5; ρ_{w} is the fluid density; and y_6, y_5 are the vertical coordinates of Node 6 and Node 5, respectively.

2.2.2. Constitutive model of joint element

In the calculation domain of FEM, the cohesive zone model (Dugdale, 1960; Barenblatt, 1962) is used to simulate the fracture process. It considers that there is a zone called fracture process zone (FPZ) in the fracture tip when the fracture is broken. The joint elements may yield and break in Mode I (tensile mode), Mode II (shear mode) or Mode I-II (mixed mode) under the *in-situ* stresses.

According to the model proposed by Hillerborg et al. (1976), the normal stress of the Mode I fracture increases linearly until it reaches a critical value σ_{t} in the initiation stage (Fig. 4). At this time, the corresponding normal displacement is o_{p}, the normal stress of the joint element can be expressed as:

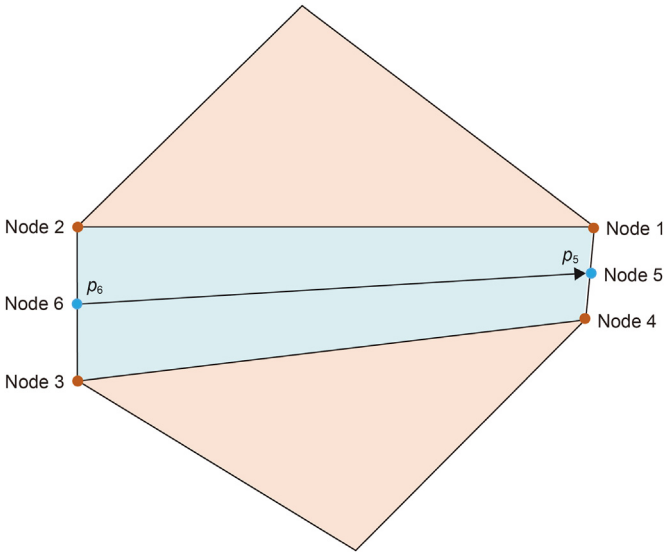

Fig. 3. Fluid flow in the joint element.

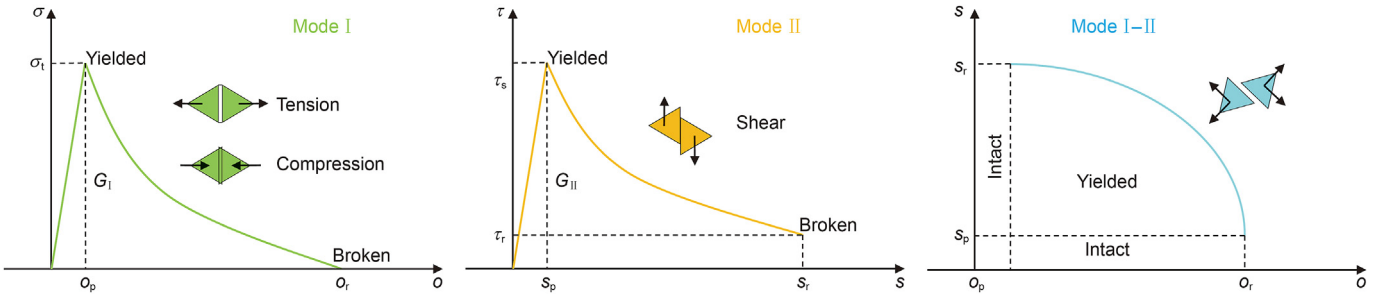

Fig. 4. Non-linear behavior of fractures with three modes.

$$\sigma = 2o\sigma_t / o_p \quad o < o_p \tag{11}$$

where σ is the normal stress of the joint elements; o is the normal displacement of the joint elements; σ_t is the tensile strength of the rock; and o_p is the normal displacement of the joint elements when the normal stress on the fracture surface is equal to the tensile strength. Then, when the cohesive stress exceeds the tensile strength, the fractures begin to enter the damaged stage, and the model proposed by Munjiza (2004) is used to describe the relationship between the stress and displacement. The normal stress of the joint element can be expressed as:

$$\sigma = \left[2o \Big/ o_p - (o/o_p)^2\right]\sigma_t \quad o_p < o < o_r \tag{12}$$

where o_r is the critical normal displacement when the fracture is broken. After that, the normal stress on the fracture surface decreases to 0.

Similar to Mode I fracture, the tangential stress of the Mode II fracture increases linearly until it reaches a critical value τ_s (Fig. 4). In the initiation stage, the tangential stress of the joint element can be expressed as:

$$\tau = s\tau_s / s_p \quad s < s_p \tag{13}$$

where τ is the tangential stress of the joint elements; τ_s is the shear strength of the rock; s is the tangential displacement of the joint elements; and s_p is the tangential displacement when the tangential stress on the fracture surface is equal to the shear strength. According to the slip-weakening model proposed by Ida (1972), during the damaged stage of Mode II fracture ($s_p \le s < s_r$), the tangential stress is always equal to the shear strength. It is noted that the shear strength is a dynamic variable that follows Mohr-Coulomb criterion. In this paper, the normal stress is used to obtain the value of the shear strength, so there is:

$$\tau_s = \begin{cases} c + \sigma \cdot \tan\varphi_i & \sigma < \sigma_t \\ c + \sigma_t \cdot \tan\varphi_i & \sigma \ge \sigma_t \end{cases} \tag{14}$$

where c is internal cohesion of the rock; φ_i is the internal friction angle of the rock. As the joint elements sustain further slip beyond s_r, the fracture is broken and the tangential stress becomes equal to a purely frictional resistance τ_f. And τ_f can be defined as:

$$\tau_f = \sigma \cdot \tan\varphi_f \tag{15}$$

where φ_f is the friction angle of the joint element.

Apart from Mode I and Mode II, fractures may occur mixed Mode I-II behavior. Although the normal displacement o and tangential displacement s may be less than o_r and s_r respectively, the total displacement can be quite large. Because the shear strength of Mode I fracture is related to normal stress, when the o and s satisfy the following coupling relationship, the mixed failure of the joint elements occurs:

$$\left(\frac{o - o_p}{o_r - o_p}\right)^2 + \left(\frac{s - s_p}{s_r - s_p}\right)^2 \ge 1 \tag{16}$$

In this paper, fracture energy is used to characterize the complete failure of fractures. The tensile fracture energy and shear fracture energy can be expressed as:

$$\begin{cases} G_I = \int_{o_p}^{o_r} \sigma(o)\mathrm{d}o \\ G_{II} = \int_{s_p}^{s_r} \left[\sigma(r) - \tau_f\right]\mathrm{d}r \end{cases} \tag{17}$$

where G_I is the tensile fracture energy and G_{II} is the shear fracture energy. And a quadratic energy criterion is used to judge the complete failure of fractures (Hutchinson et al., 1991):

$$D = \sqrt{\left(\frac{G_I}{G_{IC}}\right)^2 + \left(\frac{G_{II}}{G_{IIC}}\right)^2} \tag{18}$$

where G_{IC} and G_{IIC} are the critical tensile fracture energy and critical shear fracture energy, respectively; and D is the fracture damage index with a value between 0 and 1. When D increases to 1, the normal and tangential stress of the joint elements reduce to 0.

2.2.3. Deformation of the rock mass

In addition to the *in-situ* stress, in the process of the fracture propagation, the rock mass (that is, the fracture surface) is also subjected to the cohesive stress and fluid pressure exerted by the fluid. So, under the combined action of the above stresses, the rock will deform. In this paper, the rock is assumed to only occur elastic deformation. According to Hooke's law, the stress and strain relationship of the rock can be expressed as:

$$\boldsymbol{\sigma} = \mathbf{D}e(\mathbf{u}) \tag{19}$$

where $\boldsymbol{\sigma}$ is the total stress; $\mathbf{D}$ is the elastic parameter matrix; $e(\mathbf{u})$ is the linear strain; and $\mathbf{u}$ is the node displacement.

Meanwhile, the stress balance equation of the rock mass is:

$$-\nabla \cdot \boldsymbol{\sigma} = 0 \tag{20}$$

Under the initial conditions, only the pre-applied *in-situ* stress is applied to the rock mass, so the initial stress and strain state is:

$$\begin{cases} \boldsymbol{\sigma}_{t=0} = \boldsymbol{\sigma}_0 \\ \tau_{xy,\mathbf{u}=0} = 0 \end{cases} \tag{21}$$

where $\boldsymbol{\sigma}_0$ is the initial *in-situ* stress; and τ_{xy} is the tangential strain.

The displacement boundary is used for the outer boundary condition of the model:

$$\begin{cases} \mathbf{u}_x = 0|_{x=x_0}, \quad \mathbf{u}_x = 0|_{x=x_{\text{side}}} \\ \mathbf{u}_y = 0|_{y=y_0}, \quad \mathbf{u}_y = 0|_{y=y_{\text{side}}} \end{cases} \tag{22}$$

where x_{side} is the geometry boundary in the x direction, and y_{side} is the geometry boundary in the y direction.

2.3. Model verification

It is generally believed that two dissipative processes exist in the propagation of the fluid-driven fracture: fracturing of the rock (toughness) and dissipation in the fracturing fluid (viscosity). The energy dissipated in viscous flow is dominated under the geomechanical conditions of deep oil and gas reservoirs, even if the fluid viscosity is low. A viscosity-dominated KGD analytical model is chosen to verify our FEM-DFN model. Since the plane-strain fracture of the KGD model is symmetrical, we established a symmetrical model with a size of 120 mm × 120 mm accordingly (Fig. 5). The flow in the rock matrix is ignored and only the elastic deformation of rock is considered. A precast fracture with a length of 20 mm is set at the center of the model. The input parameters are shown in Table 1.

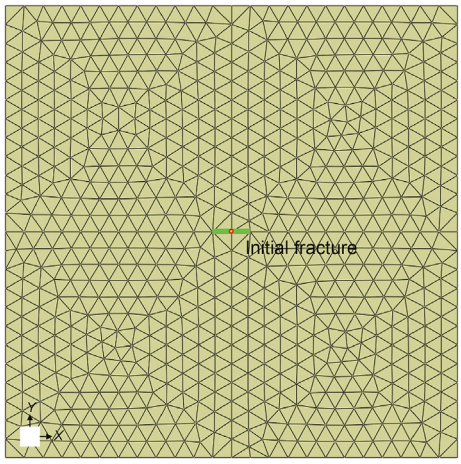

Fig. 5. The mesh model for verification.

Table 1
The input parameters for model verification.

Pumping rate, m^2/s	Pumping time, s	Fluid viscosity, mPa s	Elastic modulus, GPa	Poisson's ratio
0.001	10	1	26	0.2

The numerical solutions are compared with the analytical solutions in terms of net pressure and fracture width. The analytical expressions of the KGD model are listed in the literature of Detournay (2004). Fig. 6 compares the results calculated by FEM-DFN model and the 2D analytical solution separately. A good agreement can be obviously observed between them, which could verify the accuracy of our model to the fracture propagation problem.

3. Numerical results and discussion

3.1. The FEM-DFN model for intersection and propagation of multi-cluster fractures of Shahejie shale oil reservoir

The Jiyang Depression, located in the northeastern Shandong Province and the south eastern Bohai Bay Basin, is extremely rich in shale oil resources (Fig. 7). The Shahejie (Es) Formation is the main source rock layer in the Jiyang Depression, and is further divided into four members (Es1-4). The main lithology of Shahejie Formation is calcareous mudstone which includes a large number of laminated limestone interlayers (Fig. 8). In order to investigate the mechanism of fracture height growth, a two dimensional model including nine small layers in height direction is established and the parameters of the layers are shown in Table 2.

Fig. 9 shows the fracturing numerical model with a size of 80 m × 50 m. Four clusters are arranged on the horizontal wellbore and the cluster spacing is 10 m. In the model, bedding planes are mechanically modeled as discontinuous bedding fractures. The input parameters are shown in Table 3.

3.2. Adaptability analysis of variable fluid-viscosity fracturing

The fracture growth in fracturing treatment is largely determined by fracturing fluid viscosity. In this subsection, variable

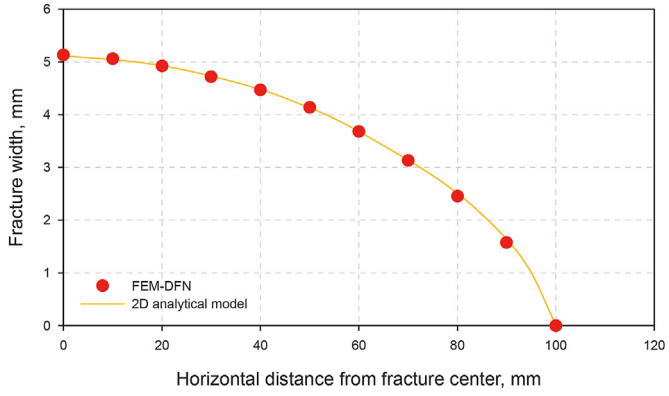

(a) Fracture width along the horizontal direction starting from the fracture center

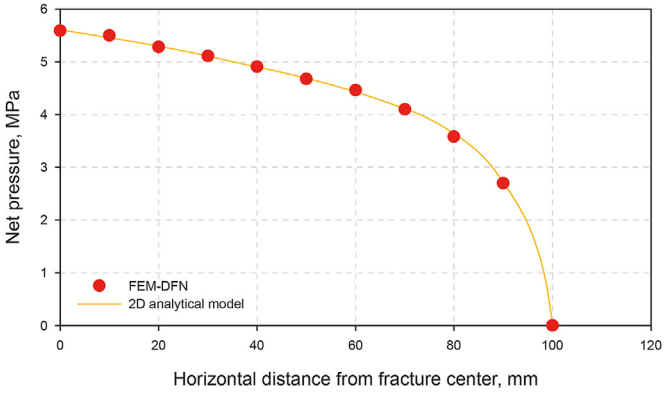

(b) Net pressure along the horizontal direction starting from the fracture center

Fig. 6. Comparison between the FEM-DFN and the analytical results.

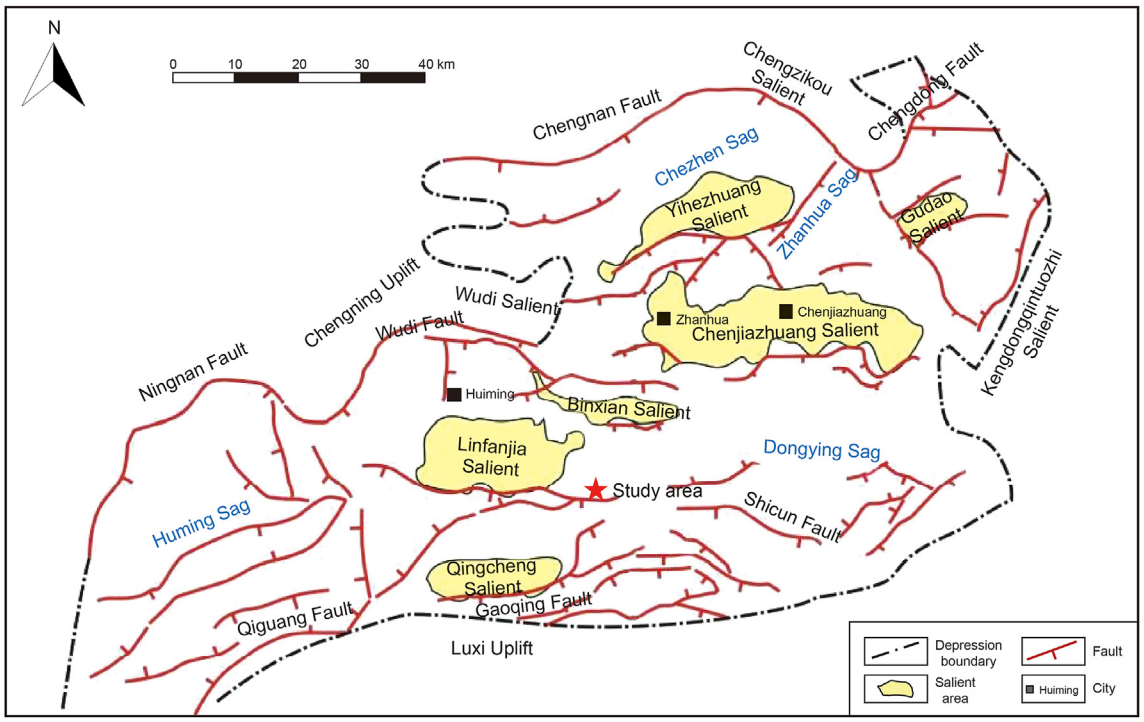

Fig. 7. The location of the Jiyang Depression in Bohai Bay Basin (modified from He et al., 2016).

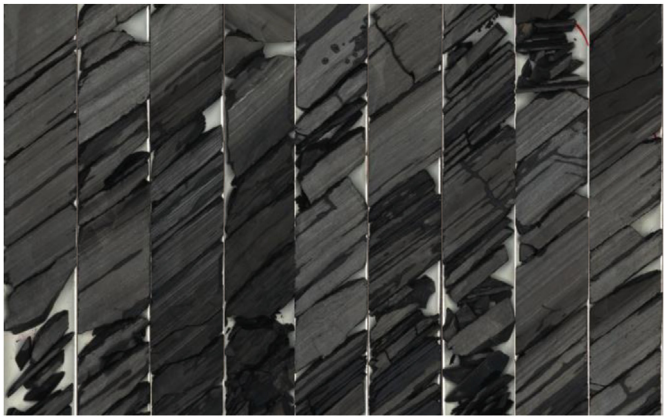

Fig. 8. The main lithology of Shahejie Formation.

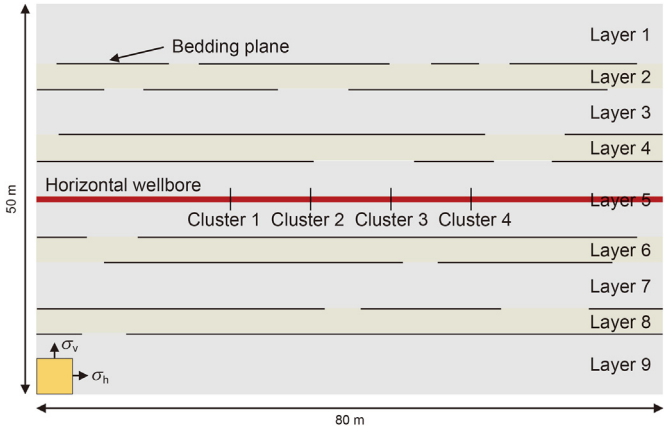

Fig. 9. The geometric model of fracture height growth in a layered reservoir.

Table 2
The layer parameters in the model.

No.	Thickness, m	Lithology	Minimum horizontal stress, MPa	Vertical stress, MPa	Elastic modulus, GPa	Poisson's ratio
1	8	Mudstone	66.0	81.0	33.22	0.214
2	3	Limestone	64.0	81.5	40.55	0.202
3	6	Mudstone	68.4	82.0	33.22	0.214
4	3	Limestone	72.5	82.5	40.55	0.202
5	10	Mudstone	65.0	83.0	33.22	0.214
6	3	Limestone	64.8	83.5	40.55	0.202
7	6	Mudstone	66.7	84.0	33.22	0.214
8	3	Limestone	69.0	84.5	40.55	0.202
9	8	Mudstone	67.0	85.0	33.22	0.214

Table 3
The parameters of the basic model.

Object	Parameter	Value
Rock mass	Normal stiffness, GPa/m	300
	Shear stiffness, GPa/m	5000
	Tensile strength, MPa	3
	Shear strength, MPa	50
	Normal fracture energy, J/m^2	10
	Shear fracture energy, J/m^2	500
	Density, kg/m^3	2500
	Friction coefficient	0.6
Bedding planes	Normal stiffness, GPa/m	300
	Shear stiffness, GPa/m	3000
	Tensile strength, MPa	0.3
	Shear strength, MPa	5
	Normal fracture energy, J/m^2	3
	Shear fracture energy, J/m^2	10
	Friction coefficient	0.4

Table 4
Fracturing fluid type and viscosity.

Case number	Fracturing fluid type	Fracturing fluid viscosity, mPa s
1	Constant viscosity	4
2	Constant viscosity	42
3	Variable viscosity	4-10.5-21-33-42

fluid-viscosity fracturing and conventional fracturing are compared to investigate their adaptability in the layered reservoir of Shengli Oilfield. As shown in Table 4, three viscosities (including variable viscosity and constant viscosity) have been selected in order to compare their difference in the height growth of multi-cluster fractures. And constant viscosity fracturing fluid includes low viscosity and high viscosity, and their values are the upper and lower limits of variable viscosity fracturing fluid, respectively. In the simulations, the pumping rate is 13 m^3/min, the cluster spacing is 10 m and the cluster number is 4.

Fig. 10 shows the model displacement field under different viscosities. It can be intuitively observed that the hydraulic fractures tend to propagate along the bedding planes when the fluid viscosity is 4 mPa s. It makes the fractures propagate farther in the direction of the minimum horizontal principal stress, but there are more non-activated areas between adjacent clusters. As the viscosity increases to 42 mPa s, it becomes easier for fractures to cross through the bedding planes directly. And when the variable viscosity is used, the propagation pattern of the multi-cluster fractures is between that with the viscosity of 4 and 42 mPa s. In addition, the fracture width of variable viscosity is generally wider than that of constant viscosity.

To further compare the differences among the three cases, the fracture geometries are obtained (Fig. 11). In Fig. 11, the propagation path of the hydraulic fractures and the interaction with bedding planes can be identified accurately. When the hydraulic fractures propagate along the height direction, it mainly forms tensile fracture; while when the hydraulic fractures encounter the bedding planes, a large number of shear fractures form in the bedding planes and their vicinity. The mixed existence of tensile fractures and shear fractures can form a complex fracture network in the reservoir. Comparing different clusters under the same viscosities, it can be observed that there are obvious differences in fracture length and width, which indicates the interference between each cluster.

In addition, L_f, L_t and L_s in Fig. 11 represent the total fracture length, tensile fracture length and shear fracture length, respectively. When the viscosity is 42 mPa s, the leak-off of the fracturing fluid to the bedding planes decreases, the increase in fluid pressure within the bedding planes slows down, and the resistance to shear slip increases, which makes it easier for the hydraulic fractures to cross through the bedding planes. It can be seen that the case with high viscosity fluid has the maximum tensile fracture length among the three cases. When a variable viscosity fracturing fluid is used, it is difficult for the hydraulic fractures to cross through the bedding planes in the low viscosity stage. Therefore, the fluid pressure is more used to increase the fracture width and activate natural fractures. Then, in the high viscosity stage, the fracture becomes easier to cross through the bedding planes. As a result, a complex fracture network combined with main fractures with sufficient height and complex branch fractures can be formed by the use of variable viscosity fracturing fluid.

3.3. Parametric analysis of growth of multi-cluster fractures

In this section, we did sensitivity analysis of fracturing fluid viscosity, pumping rate and cluster spacing, and investigated their impacts on the geometry of multi-cluster fractures and fracture

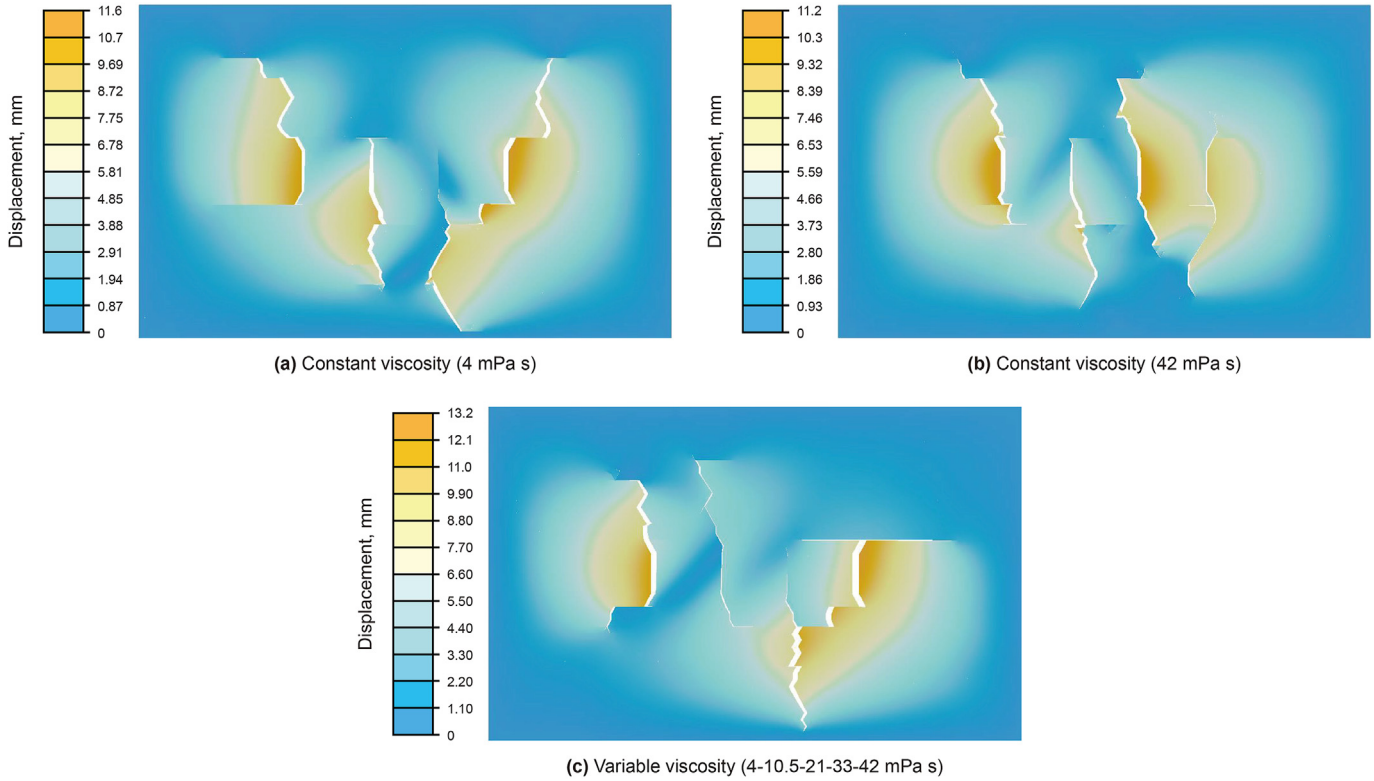

Fig. 10. The model displacement field with constant viscosity and variable viscosity.

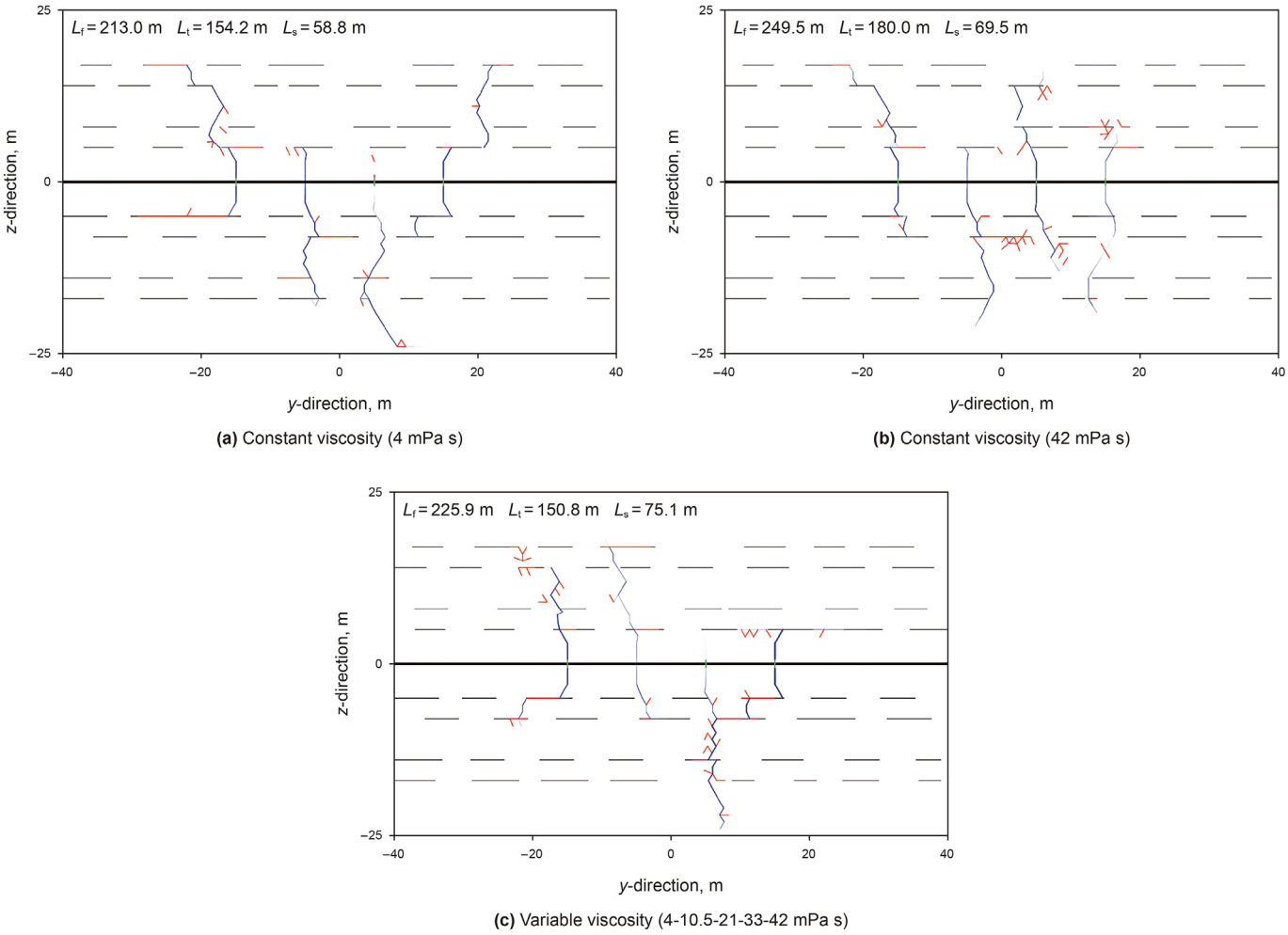

Fig. 11. The fracture geometries with constant viscosity and variable viscosity (The blue, red, and black lines represent tensile fractures, shear fractures and bedding planes, respectively).

Table 5
Different combination schemes of fluid viscosity.

Case number	Viscosity, mPa s	The degree of viscosity difference
1	5-12-21-30-39	Small
2	4-10.5-21-33-42	Medium
3	3-9-21-36-45	Large

length.

3.3.1. Fracturing fluid viscosity

The viscosity of fracturing fluid often has a range value in the fracturing treatment. Especially for high-viscosity fracturing fluids, the range is larger. Therefore, it is necessary to change the viscosity of each fluid in variable fluid-viscosity fracturing and investigate its effect on height growth of multi-cluster fractures. As shown in Table 5, from Case 1 to Case 3, the difference value of fracturing fluid viscosity in each stage gradually increases. Other required parameters are consistent with those in Section 3.2.

Previous research indicates that the stress interference between multi-fractures could make the width of the inner fractures smaller and the width of the outer fractures larger. However, it can be observed in Fig. 12(a) that the fracture width of cluster 1 and cluster 2 is larger than that of cluster 3 and cluster 4. This is because in the layered reservoir, the geometry of multi-fractures is affected by the stress interference between fractures and the distribution of bedding planes. This phenomenon of uneven propagation among multiple clusters is still obvious in the case of medium viscosity difference (Fig. 12(b)). When the viscosity difference in different stages is large (Fig. 12(c)), a more uniform fracture width can be observed. In order to more effectively compare the differences between the three cases, the fracture geometries are also obtained.

As shown in Fig. 13, only when the viscosity difference is large can each cluster have ideal fracture height at the same time. In high viscosity stage, larger fluid viscosity makes it easier for fractures to obtain stronger crossing ability in the height direction. Moreover, the fracture has maximum total length at high viscosity difference. This indicates that appropriately large viscosity difference in different viscosity stages is the better treatment strategy for variable fluid-viscosity fracturing. Comparing the three cases, the viscosity of 3-9-21-36-45 mPa s is better for the height growth of multi-cluster fractures.

3.3.2. Pumping rate

It is clear that different pumping rates provide different pressures within fractures to overcome the resistance encountered the bedding planes. In other words, different pumping rates can result in different fracture geometries. The pumping rate in the fracturing treatment of shale oil well in the Shengli Oilfield is about 13–15 m^3/min. So, in our simulations, the pumping rate is taken as 11, 13, 15,

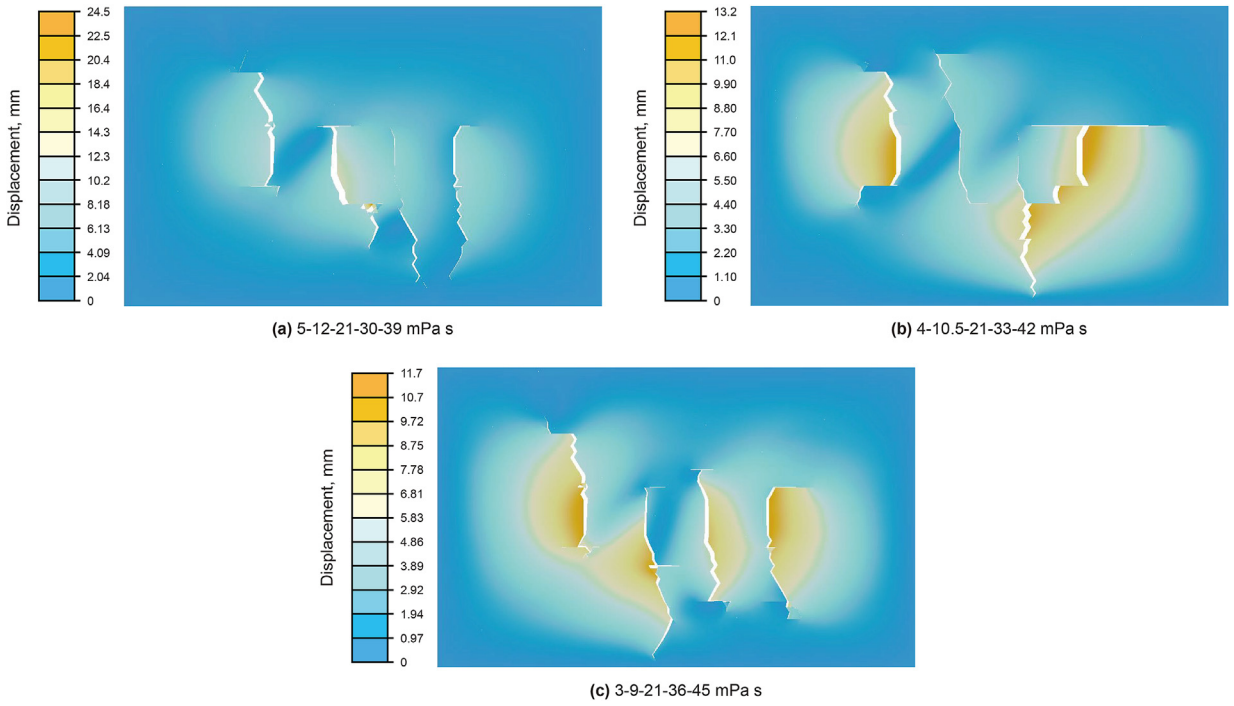

Fig. 12. The model displacement field with fracturing fluids of different viscosities.

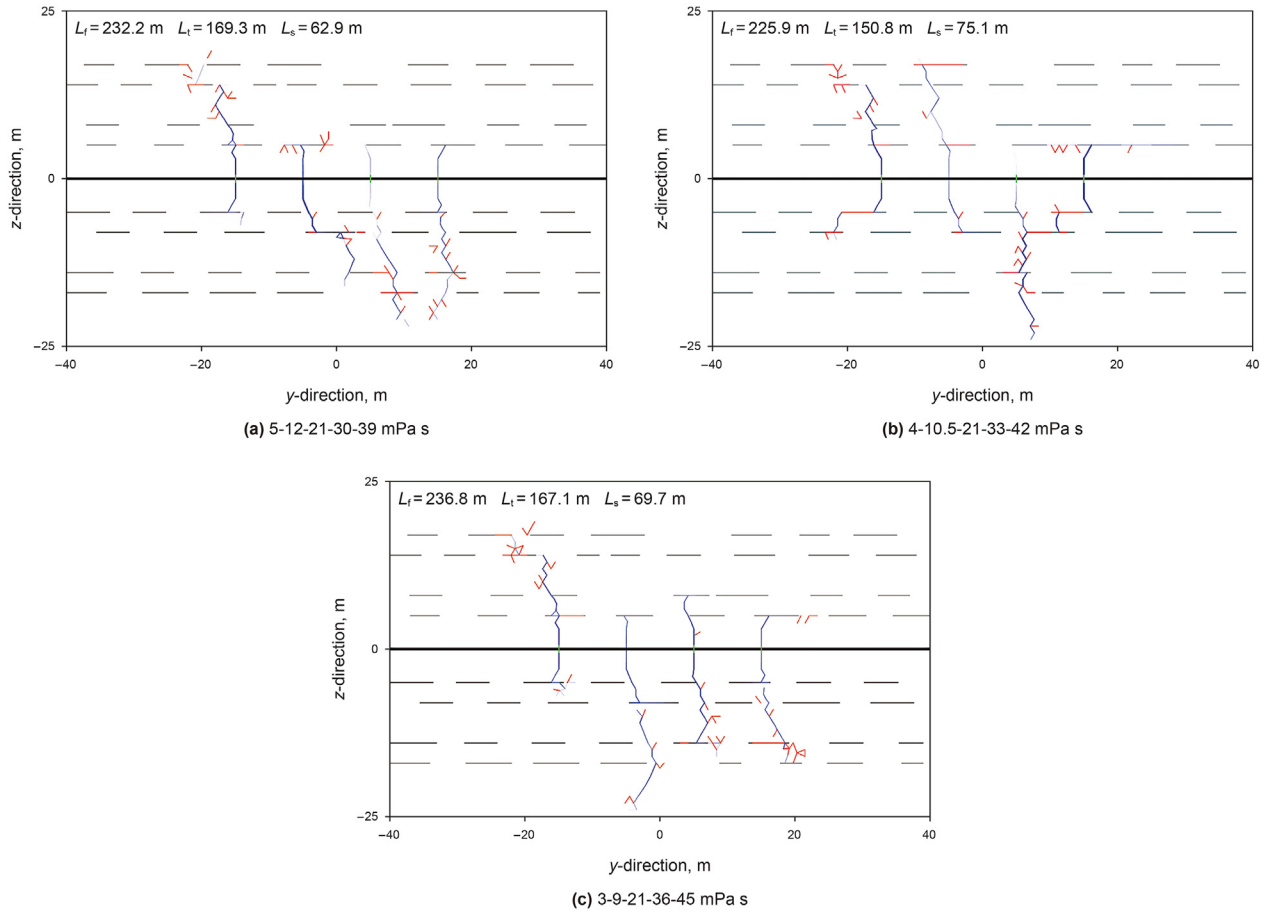

Fig. 13. The fracture geometries with fracturing fluids of different viscosities.

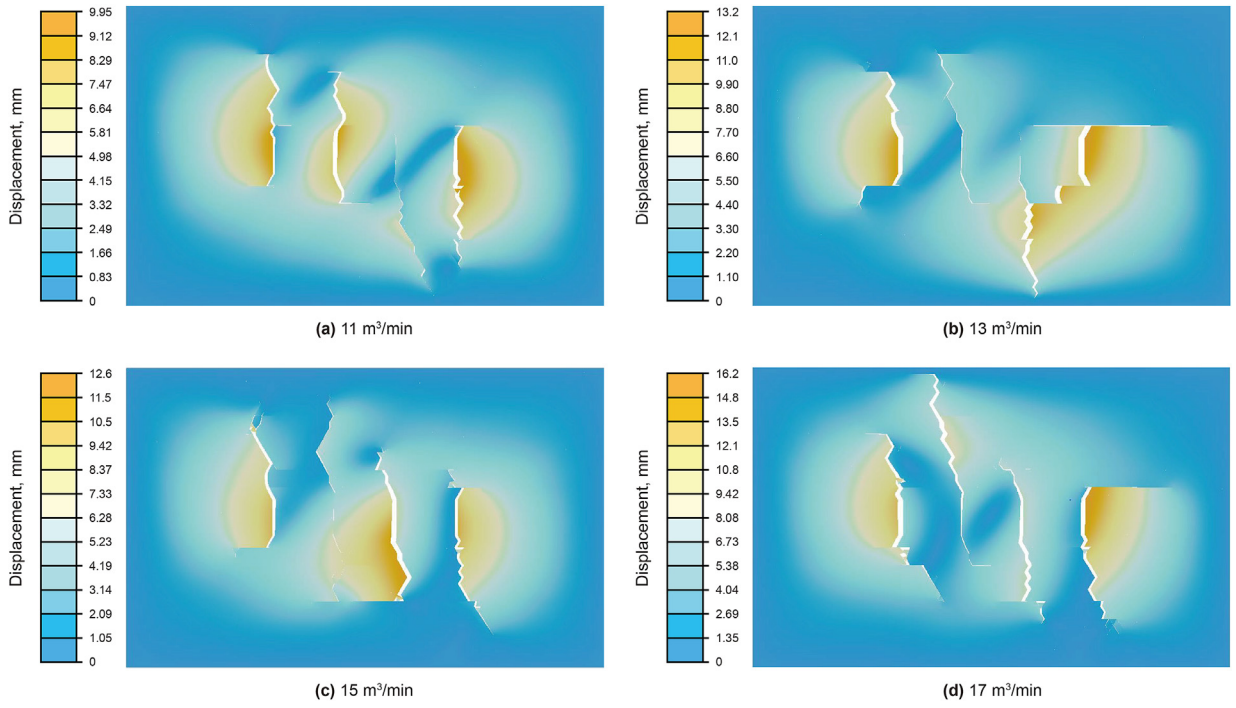

Fig. 14. The model displacement field under different pumping rates.

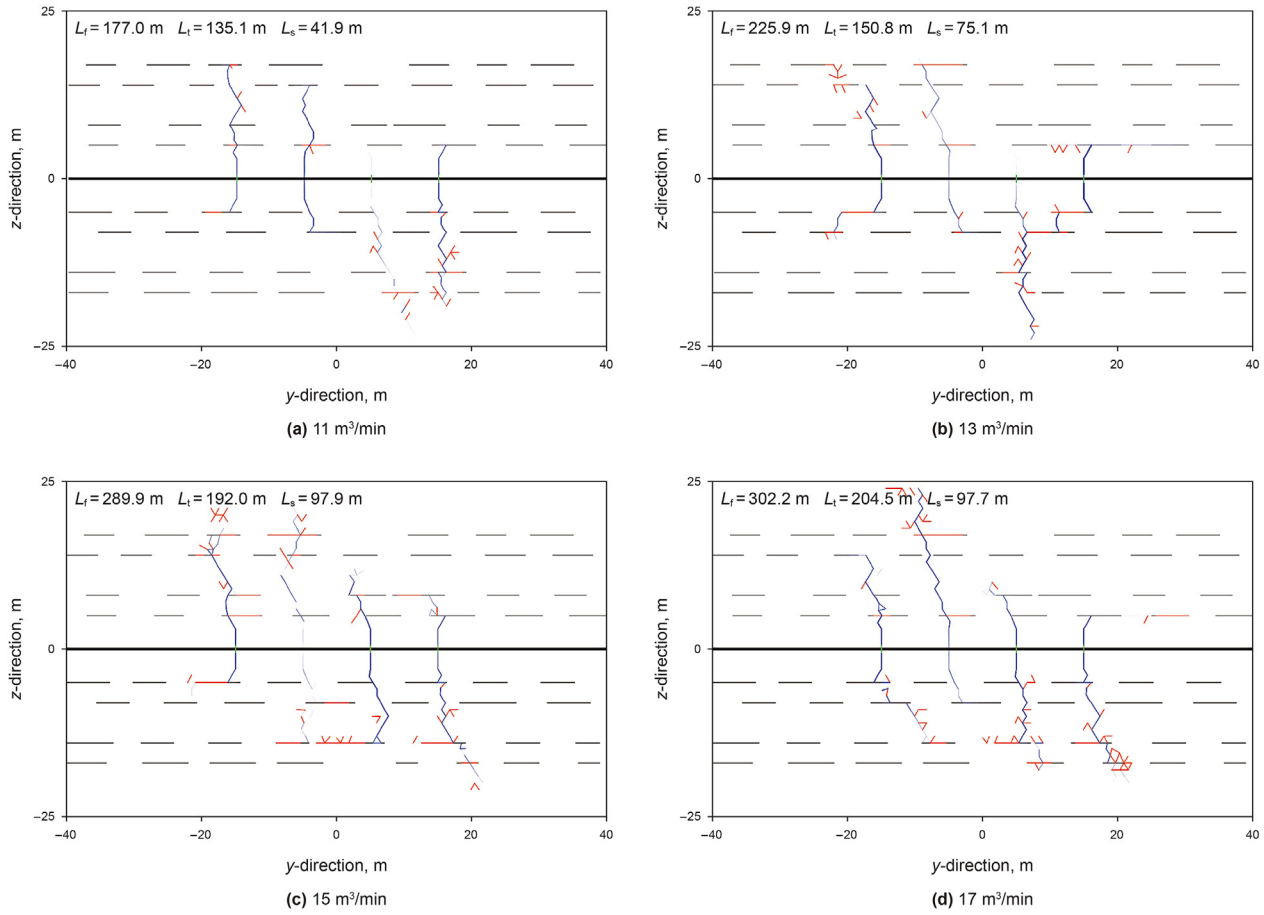

Fig. 15. The fracture geometries under different pumping rates.

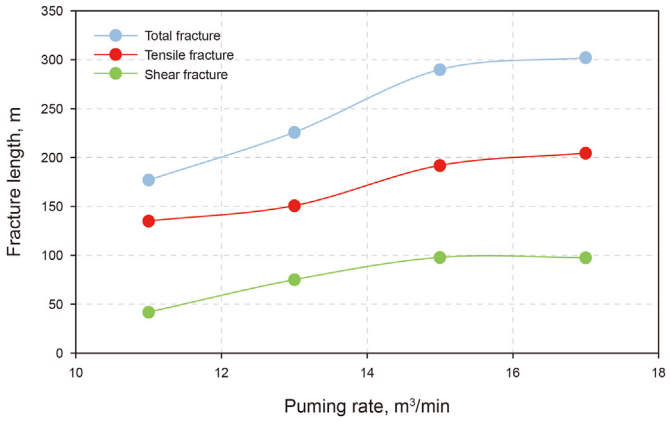

Fig. 16. The fracture length under different pumping rates.

and 17 m^3/min in four cases. The other parameters keep the same as the basic model. The model displacement field of the four cases is shown in Fig. 14. The results illustrate that a higher pumping rate contributes to a larger fracture height in general. The larger pore pressure makes it easier for the hydraulic fractures to cross through the bedding planes.

The fracture geometries can show the differences under different pumping rates clearly (Fig. 15). When hydraulic fractures encounter bedding planes, they basically stop propagating directly under pumping rate of 11 m^3/min. So, it is difficult for main fractures to wake bedding planes so as to generate shear fractures. With the gradual increase in pumping rate, more fractures can continue to propagate along the bedding planes, which makes the total fracture length increase markedly. When the pumping rate reaches 17 m^3/min, part of the fractures can propagate to the model boundary. However, by comparing the fracture length under the four pumping rates (Fig. 16), it can be observed that although the increase in pumping rate can increase the total fracture length, when the pumping rate is higher than 15 m^3/min, the increase range becomes smaller.

3.3.3. Cluster spacing

Cluster spacing markedly affects the strength of stress interference during the propagation of multi-cluster fractures. The cluster spacing in the fracturing treatment of shale oil reservoir in the Shengli Oilfield is about 6–16 m. In our simulations, the cluster spacing is taken as 15, 10, 7.5, and 6 m in four cases. And in order to keep the stage length constant, the cluster numbers of the four cases are 3, 4, 5, and 6, respectively. The other parameters keep the same as the basic model. The model displacement field of the four cases is shown in Fig. 17. When the cluster spacing is 15 m, the three clusters can propagate to the model boundary on one side of the wellbore almost in a balanced way. With the decrease in the cluster spacing, the stress interference among clusters increases markedly, which leads to the limitation of the fracture width of some clusters. When the cluster spacing reduces to 6 m, the overall fracture width becomes worse compared with the large cluster spacing.

Fig. 18 shows the fracture geometries of multi-cluster fractures with the given cluster spacings. The fractures mainly propagate on one side of the wellbore under the condition of cluster spacing of 15 m. On this side, the fractures can cross through the bedding planes or continue to propagate in the height direction at the end of the bedding planes. However, the complexity of fracture network in the model is relatively small. With the decrease in the cluster spacing, the average flow rate in each fracture decreases, which leads to the limited growth of fracture height and the smaller fracture width. As the cluster spacing decreases from 15 to 6 m (the number of clusters increases from 3 to 6), the tensile fracture length

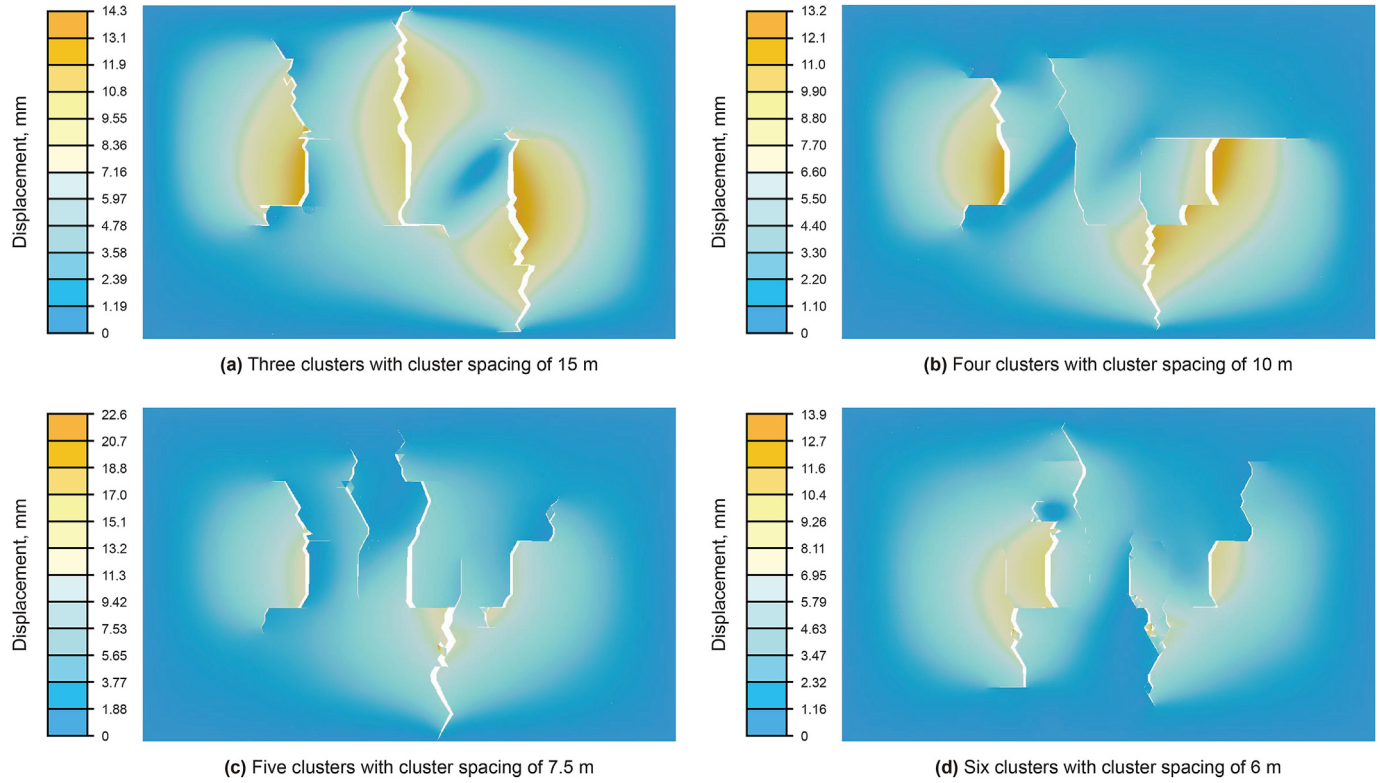

Fig. 17. The model displacement field with different cluster spacings.

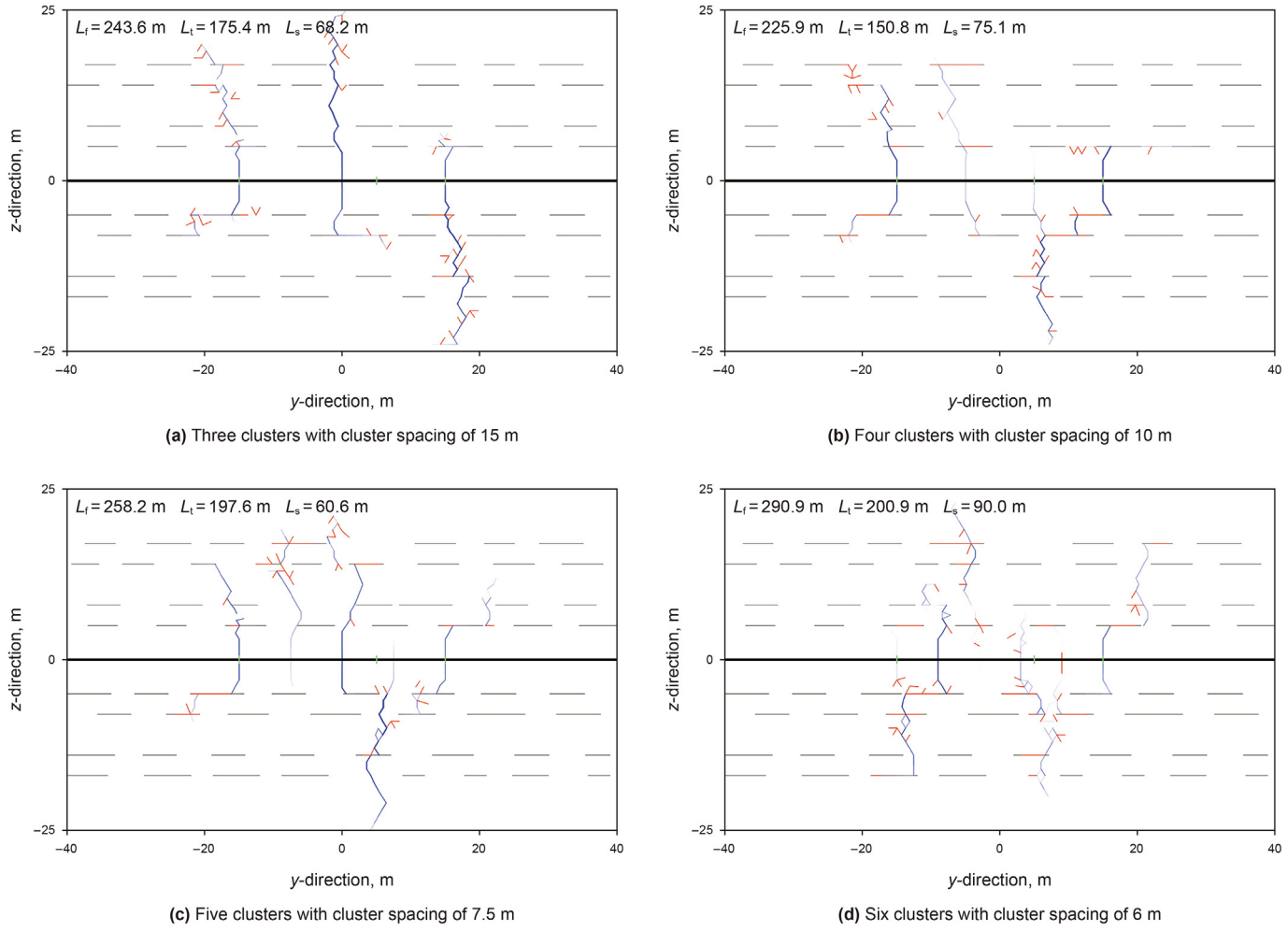

(a) Three clusters with cluster spacing of 15 m

(b) Four clusters with cluster spacing of 10 m

(c) Five clusters with cluster spacing of 7.5 m

(d) Six clusters with cluster spacing of 6 m

Fig. 18. Fracture geometries with different cluster spacings.

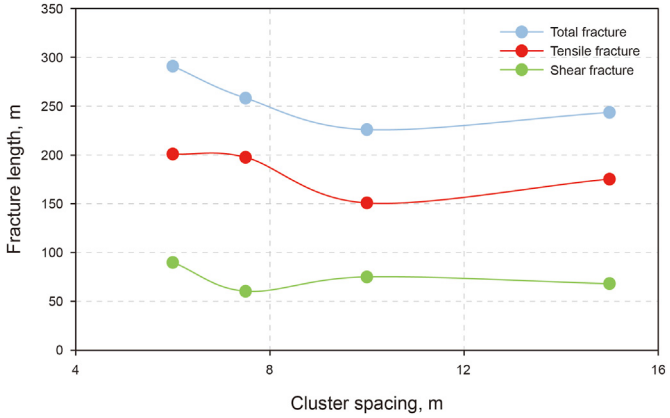

Fig. 19. The fracture length with different cluster spacings.

and the total fracture length first decrease and then increase (Fig. 19), which illustrates that small cluster spacing can increase the complexity of formation fracture network. However, small cluster spacing is not conducive to the fracture growth in the height direction. So, in order to take both the fracture height and the complexity of the fracture network into account, the cluster spacing of 7.5 m is the best choice in our simulations.

Table 6
The fluid parameters of the application well.

Fracturing fluid type	Viscosity, mPa s	Proportion of pumping time, %
Slickwater	3	29
Low viscosity fluid	9	21
Medium viscosity fluid	21	28
High viscosity fluid	36	8
Gel	45	14

4. Field application

4.1. Fracturing parameters of the application well

According to the optimization results, a field application has been implemented in a typical shale oil horizontal well whose main producing layer is Es4 member. The well has a total depth of 5364 m and a horizontal section length of 1694 m. It has 31 fracturing stages and each stage is 31–69 m with 4–6 clusters. The actual pumping rate is 14–16 m^3/min. The variable viscosity injection procedure was applied to the well and the parameters of the fracturing fluids are listed in Table 6.

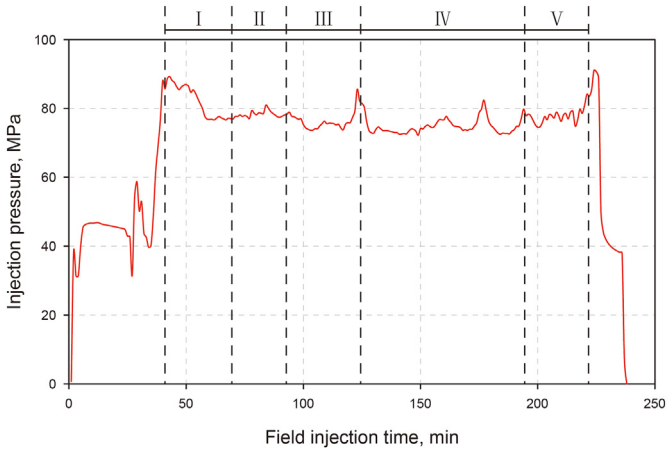

Fig. 20. The field injection pressure curves during variable fluid-viscosity fracturing of the application well, stage 15.

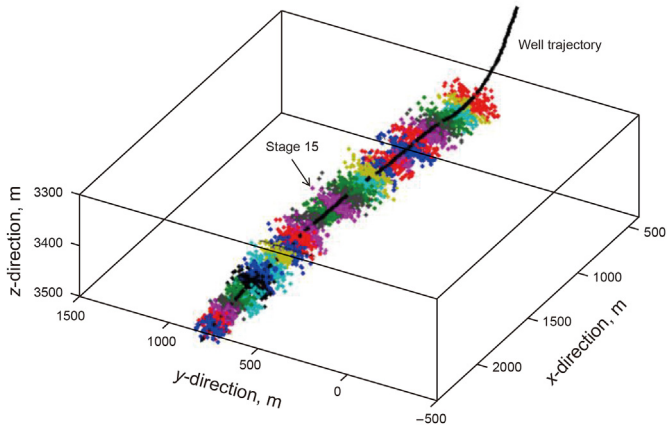

Fig. 21. The processed field microseismic events of the application well.

4.2. Results of hydraulic fracturing treatment

Fig. 20 shows the pressure curves in the fracturing treatment of the well, stage 15. In Fig. 20, the stage I, II, III, IV, and V represent five fracturing fluids, respectively. The microseismic monitoring results of the well shows that the length, width, and height of the fracture network of the fracturing stage are 306, 64, and 36 m, respectively (Fig. 21). The SRV of the stage is 47.12 $\times$ 10^4 m^3. The above data shows that the variable fluid-viscosity fracturing has achieved the dual purpose of improving the complexity of fracture network and fracture height.

The peak oil production of the application well after fracturing treatment reached 171 t/day (2.85 times that of the adjacent well), which is the highest daily production record of a single shale oil well in China, marking a strategic breakthrough of commercial shale oil production in the Jiyang Depression, Shengli Oilfield. After half a year of production, the average oil production could still stably maintain at about 28 t/day. The results illustrate that the variable fluid-viscosity fracturing can greatly improve the well production of shale oil reservoir.

5. Conclusions

A FEM-DFN model is developed to investigate the interaction and propagation of multi-cluster fractures during variable fluid-viscosity injection in layered shale oil reservoirs. The main conclusions include:

(1) Compared with conventional constant fluid-viscosity fracturing, variable fluid-viscosity injection can simultaneously ensure the complexity of the fracture network and the height of the main fractures. And appropriately large viscosity difference in different viscosity stages can give better play to the advantages of variable fluid-viscosity fracturing. The viscosity of 3-9-21-36-45 mPa s is better for the height growth of multi-cluster fractures.

(2) High pumping rate is more conducive to the growth of the main fractures and the activation of natural fractures. However, considering the cost of fracturing treatment, controlling the pumping rate at about 15 m^3/min could be the better treatment strategy in field application.

(3) Large cluster spacing can make main fractures grow better, but it is not conducive to improving the complexity between adjacent fractures. While small cluster spacing can make the interference between fractures too large, resulting in uneven propagation of multi-cluster fractures. Considering the complexity and uniform propagation of multi-cluster fractures, the cluster spacing of 7.5 m is a better choice in this study.

(4) Based on the optimized treatment parameters, variable fluid-viscosity fracturing has carried out in an oil shale well in the Shengli Oilfield. The results illustrate that the variable fluid-viscosity technique can greatly improve the stimulated reservoir volume and production of shale oil well.

Acknowledgments

This work was funded by the National Natural Science Foundation of China (Nos. 52192622, 51874253, U20A202). The authors also sincerely thank the editors and the reviewers for their efforts in improving this article.

References

Aimene, Y., Hammerquist, C., Ouenes, A., 2019. Anisotropic damage mechanics for asymmetric hydraulic fracture height propagation in a layered unconventional gas reservoir. J. Nat. Gas Sci. Eng. 67, 1–13. https://doi.org/10.1016/j.jngse.2019.04.013.

Barenblatt, G.I., 1962. The mathematical theory of equilibrium cracks in brittle fracture. Adv. Appl. Mech. 7, 55–129. https://doi.org/10.1016/S0065-2156(08)70121-2.

Bunger, A.P., Kear, J., Jeffrey, R.G., et al., 2015. Laboratory investigation of hydraulic fracture growth through weak discontinuities with active ultrasound monitoring. In: 13th ISRM International Congress of Rock Mechanics. Paper Number: ISRM-13CONGRESS-2015-174.

Detournay, E., 2004. Propagation regimes of fluid-driven fractures in impermeable rocks. Int. J. GeoMech. 4 (1), 35–45. https://doi.org/10.1061/(ASCE)1532-3641(2004)4:1(35).

Dugdale, D.S., 1960. Yielding of steel sheets containing slits. J. Mech. Phys. Solid. 8, 100–108. https://doi.org/10.1016/0022-5096(60)90013-2.

Guo, J., Luo, B., Lu, C., et al., 2017. Numerical investigation of hydraulic fracture propagation in a layered reservoir using the cohesive zone method. Eng. Fract. Mech. 186, 195–207. https://doi.org/10.1016/j.engfracmech.2017.10.013.

Guo, J., Lu, Q., Chen, H., et al., 2018. Quantitative phase field modeling of hydraulic fracture branching in heterogeneous formation under anisotropic in-situ stress. J. Nat. Gas Sci. Eng. 56, 455–471. https://doi.org/10.1016/j.jngse.2018.06.009.

Guo, T., Wang, X., Li, Z., et al., 2019. Numerical simulation study on fracture propagation of zipper and synchronous fracturing in hydrogen energy development. Int. J. Hydrogen Energy 44 (11), 5270–5285. https://doi.org/10.1016/j.ijhydene.2018.08.072.

He, J., Ding, W., Jiang, Z., et al., 2016. Logging identification and characteristic analysis of the lacustrine organic-rich shale lithofacies: a case study from the Es_3^1 shale in the Jiyang Depression, Bohai Bay Basin, Eastern China. J. Petrol. Sci. Eng. 145 (1), 238–255. https://doi.org/10.1016/j.petrol.2016.05.017.

Hillerborg, A., Modéer, M., Petersson, P.E., 1976. Analysis of crack formation and crack growth in concrete by means of fracture mechanics and finite elements. Cement Concr. Res. 6 (6), 773–781. https://doi.org/10.1016/0008-8846(76)90007-7.

Hossain, M.M., Rahman, M.K., 2008. Numerical simulation of complex fracture growth during tight reservoir stimulation by hydraulic fracturing. J. Petrol. Sci. Eng. 602 (2), 86–104. https://doi.org/10.1016/j.petrol.2007.05.007.
Hutchinson, J.W., Suo, Z., 1991. Mixed mode cracking in layered materials. Adv. Appl. Mech. 29 (C), 63–191. https://doi.org/10.1016/S0065-2156(08)70164-9.
Ida, Y., 1972. Cohesive force across the tip of a longitudinal-shear crack and Griffith's specific surface energy. J. Geophys. Res. 77 (20), 3796–3805. https://doi.org/10.1029/JB077i020p03796.
Ju, Y., Wang, Y., Xu, B., et al., 2019. Numerical analysis of the effects of bedded interfaces on hydraulic fracture propagation in tight multilayered reservoirs considering hydro-mechanical coupling. J Petrol Sci Eng 178, 356–375. https://doi.org/10.1016/j.petrol.2019.03.049.
Li, D., Zhang, S., Zhang, S., 2014. Experimental and numerical simulation study on fracturing through interlayer to coal seam. J. Nat. Gas Sci. Eng. 21, 386–396. https://doi.org/10.1016/j.jngse.2014.08.022.
Li, J., Liu, Y., Wu, K., et al., 2021. A new higher order displacement discontinuity method based on the joint element for analysis of close-spacing planar fractures. SPE J. https://doi.org/10.2118/208614-PA.
Li, N., Zhang, S., Zou, Y., et al., 2018. Experimental analysis of hydraulic fracture growth and acoustic emission response in a layered formation. Rock Mech. Rock Eng. 51 (4), 1047–1062. https://doi.org/10.1007/s00603-017-1383-z.
Lu, C., Li, M., Guo, J., et al., 2015. Engineering geological characteristics and the hydraulic fracture propagation mechanism of the sand-shale interbedded formation in the Xu5 reservoir. J. Geophys. Eng. 12 (3), 321–339. https://doi.org/10.1088/1742-2132/12/3/321.
Miehe, C., Hofacker, M., Schänzel, L.M., 2015. Phase field modeling of fracture in multi-physics problems. Part II. Coupled brittle-to-ductile failure criteria and crack propagation in thermo-elastic-plastic solids. Comput. Methods Appl. Math. 294, 486–522. https://doi.org/10.1016/j.cma.2014.11.017.
Munjiza, A., 2004. The Combined Finite-Discrete Element Method. John Wiley & Sons Ltd, Chichester, West Sussex, England.
Rahman, M.M., Hossain, M.M., Crosby, D.G., et al., 2002. Analytical, numerical and experimental investigations of transverse fracture propagation from horizontal wells. J. Petrol. Sci. Eng. 35 (3), 127–150. https://doi.org/10.1016/S0920-4105(02)00236-X.
Shou, K., Napier, J.A.L., 1999. A two-dimensional linear variation displacement discontinuity method for three-layered elastic media. Int J Rock Mech Min 36 (6), 719–729. https://doi.org/10.1016/S0148-9062(99)00042-X.
Tang, J., Li, J., Tang, M., et al., 2019. Investigation of multiple hydraulic fractures evolution and well performance in lacustrine shale oil reservoirs considering stress heterogeneity. Eng. Fract. Mech. 281, 106569. https://doi.org/10.1016/j.engfracmech.2019.106569.
Tang, J., Wu, K., Zeng, B., et al., 2018. Investigate effects of weak bedding interfaces on fracture geometry in unconventional reservoirs. J. Petrol. Sci. Eng. 165, 992–1009. https://doi.org/10.1016/j.petrol.2017.11.037.
Wang, H., Liu, H., Wu, H., et al., 2015. A 3D numerical model for studying the effect of interface shear failure on hydraulic fracture height containment. J. Petrol. Sci. Eng. 133, 280–284. https://doi.org/10.1016/j.petrol.2015.06.016.
Wang, Y., Zhang, Z., 2020. Fully hydromechanical coupled hydraulic fracture simulation considering state transition of natural fracture. J. Petrol. Sci. Eng. 190, 107072. https://doi.org/10.1016/j.petrol.2020.107072.
Weng, X., Chuprakov, D., Kresse, O., et al., 2018. Hydraulic fracture-height containment by permeable weak bedding interfaces. Geophysics 83 (3), 137–152. https://doi.org/10.1190/geo2017-0048.1.
Xie, J., Tang, J., Yong, R., et al., 2020. A 3-D hydraulic fracture propagation model applied for shale gas reservoirs with multiple bedding planes. Eng. Fract. Mech. 228, 106872. https://doi.org/10.1016/j.engfracmech.2020.106872.
Zeng, Q., Liu, W., Yao, J., 2018. Hydro-mechanical modeling of hydraulic fracture propagation based on embedded discrete fracture model and extended finite element method. J. Petrol. Sci. Eng. 167, 64–77. https://doi.org/10.1016/j.petrol.2018.03.086.
Zhang, X., Jeffrey, R.G., Thiercelin, M., 2007. Deflection and propagation of fluid-driven fractures at frictional bedded interfaces: a numerical investigation. J. Struct. Geol. 29 (3), 396–410. https://doi.org/10.1016/j.jsg.2006.09.013.
Zhang, Z., Wang, D., Ge, X., 2013. A novel triangular finite element partition method for fracture simulation without enrichment of interpolation. Int J Comp Meth-Sing. 10 (4), 1350015. https://doi.org/10.1142/S0219876213500151.
Zhang, Z., Wang, D., Ge, X., et al., 2016. Three-dimensional element partition method for fracture simulation. Int. J. GeoMech. 16 (3), 04015074. https://doi.org/10.1061/(ASCE)GM.1943-5622.0000597.
Zhou, T., Wang, H., Li, F., et al., 2020. Numerical simulation of hydraulic fracture propagation in laminated shale reservoirs. Petrol. Explor. Dev. 47 (5), 1117–1130. https://doi.org/10.1016/S1876-3804(20)60122-7.
Zhu, H., Zhao, X., Guo, J., et al., 2015. Coupled flow-stress-damage simulation of deviated-wellbore fracturing in hard-rock. J. Nat. Gas Sci. Eng. 26, 711–724. https://doi.org/10.1016/j.jngse.2015.07.007, 2015.
Zhu, H., Jin, X., Guo, J., An, F., et al., 2016. Coupled flow, stress and damage modelling of interactions between hydraulic fractures and natural fractures in shale gas reservoirs. Int. J. Oil Gas Coal Technol. 13 (4), 359–390. https://doi.org/10.1504/IJOGCT.2016.10000752.
Zhu, H., Wang, H., Tang, X., et al., 2019. Hydraulic fracture propagation in sand-mudstone interbedded reservoir integrated with different fluid flow of multi-perforated fractures. In: ARMA-CUPB Geothermal International Conference. Paper Number: ARMA-CUPB-19-6836.
Zhu, H., Tang, X., Song, Y., et al., 2021. An infill well fracturing model and its microseismic events barrier effect: a case in Fuling shale gas reservoir. SPE J. 26 (1), 113–134. https://doi.org/10.2118/202485-PA, 2021.
Zou, Y., Ma, X., Zhou, T., et al., 2017. Hydraulic fracture growth in a layered formation based on fracturing experiments and discrete element modeling. Rock Mech. Rock Eng. 50 (9), 2381–2395. https://doi.org/10.1007/s00603-017-1241-z.